The process of Lewy body formation, rather than simply α-synuclein fibrillization, is one of the major drivers of neurodegeneration

Anne-Laure Mahul-Mellier[a], Johannes Burtscher[a], Niran Maharjan[a], Laura Weerens[a], Marie Croisier[b], Fabien Kuttler[c], Marion Leleu[d,e], Graham W. Knott[b], and Hilal A. Lashuel[a,1]

[a]Laboratory of Molecular and Chemical Biology of Neurodegeneration, Brain Mind Institute, Ecole Polytechnique Fédérale de Lausanne, 1015 Lausanne, Switzerland; [b]BioEM Core Facility and Technology Platform, Ecole Polytechnique Fédérale de Lausanne, 1015 Lausanne, Switzerland; [c]Biomolecular Screening Core Facility and Technology Platform, Ecole Polytechnique Fédérale de Lausanne, 1015 Lausanne, Switzerland; [d]Gene Expression Core Facility and Technology Platform, Ecole Polytechnique Fédérale de Lausanne, 1015 Lausanne, Switzerland; and [e]Swiss Institute of Bioinformatics, Ecole Polytechnique Fédérale de Lausanne, 1015 Lausanne, Switzerland

Edited by Pietro De Camilli, Yale University, New Haven, CT, and approved December 31, 2019 (received for review August 27, 2019)

Parkinson's disease (PD) is characterized by the accumulation of misfolded and aggregated α-synuclein (α-syn) into intraneuronal inclusions named Lewy bodies (LBs). Although it is widely believed that α-syn plays a central role in the pathogenesis of PD, the processes that govern α-syn fibrillization and LB formation remain poorly understood. In this work, we sought to dissect the spatiotemporal events involved in the biogenesis of the LBs at the genetic, molecular, biochemical, structural, and cellular levels. Toward this goal, we further developed a seeding-based model of α-syn fibrillization to generate a neuronal model that reproduces the key events leading to LB formation, including seeding, fibrillization, and the formation of inclusions that recapitulate many of the biochemical, structural, and organizational features of bona fide LBs. Using an integrative omics, biochemical and imaging approach, we dissected the molecular events associated with the different stages of LB formation and their contribution to neuronal dysfunction and degeneration. In addition, we demonstrate that LB formation involves a complex interplay between α-syn fibrillization, posttranslational modifications, and interactions between α-syn aggregates and membranous organelles, including mitochondria, the autophagosome, and endolysosome. Finally, we show that the process of LB formation, rather than simply fibril formation, is one of the major drivers of neurodegeneration through disruption of cellular functions and inducing mitochondria damage and deficits, and synaptic dysfunctions. We believe that this model represents a powerful platform to further investigate the mechanisms of LB formation and clearance and to screen and evaluate therapeutics targeting α-syn aggregation and LB formation.

α-synuclein | Parkinson's disease | aggregation | Lewy body | seeding

In-depth postmortem neuropathological examinations of human brains from patients with Parkinson's disease (PD) and related synucleinopathies have revealed the existence of different subtypes of pathological inclusions that are enriched in aggregated forms of α-synuclein (α-syn), including fibrils (1–6). This has led to the hypothesis that aggregation of α-syn has a primary role in the formation of the Lewy bodies (LBs) and other α-syn pathological aggregates and therefore in the pathogenesis of synucleinopathies (7). However, the molecular and cellular processes that trigger and govern the misfolding, fibrillization, LB formation, and spread of α-syn in the brain remain poorly understood.

The absence of experimental models that reproduce all of the stages of LB formation and maturation has limited our ability to decipher the different processes involved in LB formation and the contribution of these processes to the pathogenesis of PD and synucleinopathies. To address this knowledge gap, it is crucial to develop cellular and animal models that not only produce α-syn aggregates but also recapitulate the process of LB formation at the biochemical, structural, and organizational levels. This is fundamental to elucidate the key events associated with α-syn aggregation and LB formation and maturation and to correlate these events with alteration in cellular pathways and functions/dysfunctions.

Until recently, the great majority of cellular models of synucleinopathies were based on overexpression of WT or mutant α-syn alone, with other proteins, or coupled to treatment with other stress inducers (8–10). However, very few studies investigated the extent to which these aggregates reproduce the cardinal structural and organizational features of the bona fide LB (11): 1) Dense core with irradiating filaments (classical brainstem type LB) or fibrillary structure without a central core (cortical LB); 2) p62, ubiquitin (ub), and phosphorylated α-syn (pS129) immunoreactivity; and 3) the presence of membranous organelles (4, 5, 12–16). In these studies, the aggregation properties of α-syn were indirectly assessed (8, 17, 18) while characterization of the LB-like properties was mostly limited to assessing the immunoreactivity for selected LB markers (8–10). When electron microscopy (EM) was used, it clearly demonstrated that these α-syn inclusions do

NEUROSCIENCE

Significance

Although converging evidence point to α-synuclein aggregation and Lewy body (LB) formation as central events in Parkinson's disease, the molecular mechanisms that regulate these processes and their role in disease pathogenesis remain elusive. Herein, we describe a neuronal model that reproduces the key events leading to the formation of inclusions that recapitulate the biochemical, structural, and organizational features of bona fide LBs. This model allowed us to dissect the molecular events associated with the different stages of LB formation and how they contribute to neuronal dysfunctions and degeneration, thus providing a powerful platform for evaluating therapeutics targeting α-synuclein aggregation and LB formation and to identify and validate therapeutic targets for the treatment of Parkinson's disease.

Author contributions: A.-L.M.-M., J.B., N.M., L.W., G.W.K., and H.A.L. designed research; A.-L.M.-M., J.B., N.M., L.W., and M.C. performed research; A.-L.M.-M., J.B., N.M., L.W., F.K., M.L., and G.W.K. analyzed data; and A.-L.M.-M., J.B., N.M., and H.A.L. wrote the paper.

The authors declare no competing interest.

This article is a PNAS Direct Submission.

This open access article is distributed under Creative Commons Attribution-NonCommercial-NoDerivatives License 4.0 (CC BY-NC-ND).

Data deposition: The proteomic dataset has been deposited in the ProteomeXchange via the PRIDE database, Project Name: Temporal proteomic analyses of the protein contents found in the insoluble fraction of the a-synuclein PFF-treated neurons (accession no. PXD016850). The transcriptomic dataset has been deposited in the Gene Expression Omnibus (GEO) database, https://www.ncbi.nlm.nih.gov/geo (accession no. GSE142416). Higher-quality figures are available at Figshare (https://doi.org/10.6084/m9.figshare.11842389.v2).

[1]To whom correspondence may be addressed. Email: hilal.lashuel@epfl.ch.

This article contains supporting information online at https://www.pnas.org/lookup/suppl/doi:10.1073/pnas.1913904117/-/DCSupplemental.

First published February 19, 2020.

Downloaded at Palestinian Territory, occupied on December 1, 2021

www.manaraa.com

not share the compositional complexity and morphological features of the LBs (8, 19, 20), suggesting that the majority of α-syn cellular models reproduce some aspects of α-syn aggregation or fibril formation, but do not recapitulate all of the key events leading to LB formation and maturation.

Recently, it was shown that exogenously added preformed fibrils (PFFs) of α-syn can act as seeds to initiate the misfolding and aggregation of endogenous α-syn, in both cellular (21) and animal models (22), in the absence of α-syn overexpression. Although long filamentous aggregates, immunoreactive for the standard LB makers, were observed, the transition from fibrils to LB-like structures has not been reported. This suggests that the neuronal seeding model, as initially developed, is a suitable model for investigating the processes involved in fibrils formations but not LB formation.

Given that LBs have been consistently shown to have complex composition and organization and usually contain other nonproteinaceous material (lipids) (23, 24) and membranous organelles (4, 5, 12–16), we hypothesized that the transition from fibrils to LB might require time and could be driven by posttranslational modifications, structural rearrangements of the fibrils, and α-syn interaction with organelles. By extending the characterization of this neuronal seeding model from day (D) 11 to D14 to D21, we were eventually able to observe the transition from fibrils to α-syn–rich inclusions that recapitulate the biochemical, morphological, and structural features of the bona fide human LBs, including the recruitment of membranous organelles and accumulation of phosphorylated and C-terminally truncated α-syn aggregates (25–30).

By employing an integrated approach using confocal and correlative light EM (CLEM) imaging, as well as quantitative proteomic and transcriptomic analyses, we were able to investigate with spatiotemporal resolution the biochemical and structural changes associated with each step involved in LB biogenesis, from seeding to fibrillization to LB formation and maturation. Our ability to disentangle the different stages of LB formation in this model provided unique opportunities to investigate the cellular and functional changes that occur at each stage, thus paving the way for elucidating how the different events associated with LB formation and maturation contribute to α-syn–induced toxicity and neurodegeneration.

Results

α-Syn–Seeded Aggregates Share the Immunohistochemical but Not the Structural and Morphological Features of the Bona Fide LBs. To investigate the mechanisms of LB formation and maturation, we initially took advantage of a cellular seeding-based model of synucleinopathies developed by Lee and coworkers (21). We first sought to determine to what extent this model reproduces LB formation. α-Syn mouse PFFs were added to primary neuronal cultures (Fig. 1*A* and *SI Appendix*, Fig. S1 *A–F*). Once internalized into the neurons, these seeds induced endogenous α-syn to misfold and to form intracellular aggregates in a time-dependent manner (Fig. 1*A* and *SI Appendix*, Fig. S1*F*).

Consistent with previous studies, immunocytochemistry (ICC) combined with high-content imaging analysis (HCA) showed that neurons only started to exhibit α-syn–pS129$^+$ neuritic inclusions 4 d after the addition of α-syn seeds (*SI Appendix*, Fig. S3*A*). At D7, filamentous-like α-syn aggregates were observed in the dendrites (MAP2$^+$ neurites) and to some extent in the axons (Tau$^+$/MAP2$^-$ neurites) with a limited number of cell-body aggregates (Fig. 1*B* and *SI Appendix*, Fig. S3 *B*, *E*, and *G–J*). At D14, the number of filamentous aggregates continued to significantly increase in neurites but also in the neuronal cell bodies in the vicinity of the nucleus (Fig. 1*C* and *SI Appendix*, Fig. S3 *C*, *E*, and *G–F*).

The newly formed aggregates were all positive for the three well-established LB markers, p62 (Fig. 1 *D* and *E*) and ub (Fig. 1 *F* and *G*) (31), and the Amytracker tracer, a fluorescent dye that binds specifically to the β-sheet structure of amyloid-like protein aggregates (Fig. 1 *H* and *I*). Although previous studies have suggested the formation of specific morphologies (strains) of α-syn aggregates in seeding models, our ICC data revealed the formation of aggregates that are heterogeneous in size, shape, and subcellular distribution in the same population of PFF-treated neurons (Fig. 1 *B–I* and *SI Appendix*, Fig. S3 *B* and *C*). Biochemical analysis of the insoluble fraction of the PFF-treated neurons confirmed the accumulation of both truncated and high molecular weight (HMWs) α-syn species that were positively stained with a pan-synuclein antibody and with an antibody against pS129 (Fig. 1*J* and *SI Appendix*, Fig. S7), consistent with previous reports from our group (25). These insoluble fractions displayed a potent seeding activity in neuronal primary culture (*SI Appendix*, Fig. S4) and induced the formation of seeded aggregates with a morphology and a subcellular distribution similar to those formed in PFFs-treated neurons (*SI Appendix*, Figs. S3*C* and S4*B*). These findings demonstrate that the newly formed pS129$^+$ α-syn filamentous aggregates contain α-syn seeding-competent species, most likely in a fibrillar form.

To determine if the newly formed aggregates share the structural and morphological properties of the bona fide LBs observed in PD brains, we performed EM and immunogold labeling against α-syn pS129 at D14. The newly formed aggregates in neurons appear as loosely organized uniform filaments (Fig. 1 *K*, *Lower*) without significant lateral association or clustering of the fibrils in the form of inclusions. Although previous studies have referred to the α-syn aggregates formed at 11 to 14 d posttreatment with PFFs as LB-like inclusions, our ICC and EM studies, which are consistent with previous studies using the same model (21, 32, 33) and tools (e.g., antibodies and LB markers), clearly demonstrate the formation of predominantly α-syn fibrils, rather than LB-like inclusions. LBs are highly organized round structures that are composed of not only α-syn fibrils but also other proteins (34), lipids (23, 24), and membranous organelles, including lysosomal structures and mitochondria (4, 5, 13, 35, 36). The absence of such structures at D14, even though the fibrillar aggregates are immunoreactive for the classic markers used to define LBs, such as pS129, ub, and p62, suggests that these markers cannot be used to accurately distinguish between α-syn fibrillar aggregates and mature LBs.

α-Syn–Seeded Fibrillar Aggregates Rearrange into Inclusions that Morphologically Resemble to the Bona Fide Human LBs. We hypothesized that the rearrangement and transition of the newly formed α-syn fibrils into LB-like inclusions might require more time. Therefore, we investigated the structural and morphological properties of the newly formed aggregates over an extended period, up to D21 posttreatment with PFFs. Interestingly, at D21, ICC combined with an HCA approach showed a significant increase in the number of aggregates detected in the neuronal cell bodies compared to D14 (*SI Appendix*, Fig. S3 *F–H*). Furthermore, while the seeded aggregates, up to D14, were exclusively detected as long filamentous-like structures located either in the neurites or the neuronal cell bodies (*SI Appendix*, Fig. S3 *B* and *C*), at D21 we identified three different morphologies: Filamentous (~30%), ribbon-like (~45%), and round LB-like inclusions (~22%) (*SI Appendix*, Fig. S3 *D* and *E*). The α-syn rounded inclusions observed at D21 have not been reported, as previous studies limited their analysis up to D14. They were all positive for p62, ub, the Amytracker dye (Fig. 1 *L–O*), and for several classes of lipids (*SI Appendix*, Fig. S3 *K–P*) that have been found in the bona fide LBs (16, 23, 24, 37–39). As observed in different synucleinopathies, the LB-like inclusions formed in the neuronal cell bodies were not the most abundant population of α-syn aggregates in comparison to the abundance of the filamentous inclusions formed in the neurites (40).

Finally, the LB-like inclusions were exclusively detected in the vicinity of the nucleus (Fig. 1 *L–O* and *SI Appendix*, Fig. S3 *D* and *E*). After D14, no further significant accumulation of α-syn aggregates was observed in the neurites (*SI Appendix*, Fig. S3*G*). Altogether, our data suggest that α-syn fibrillar aggregates initially

Downloaded at Palestinian Territory, occupied on December 1, 2021
www.manaraa.com

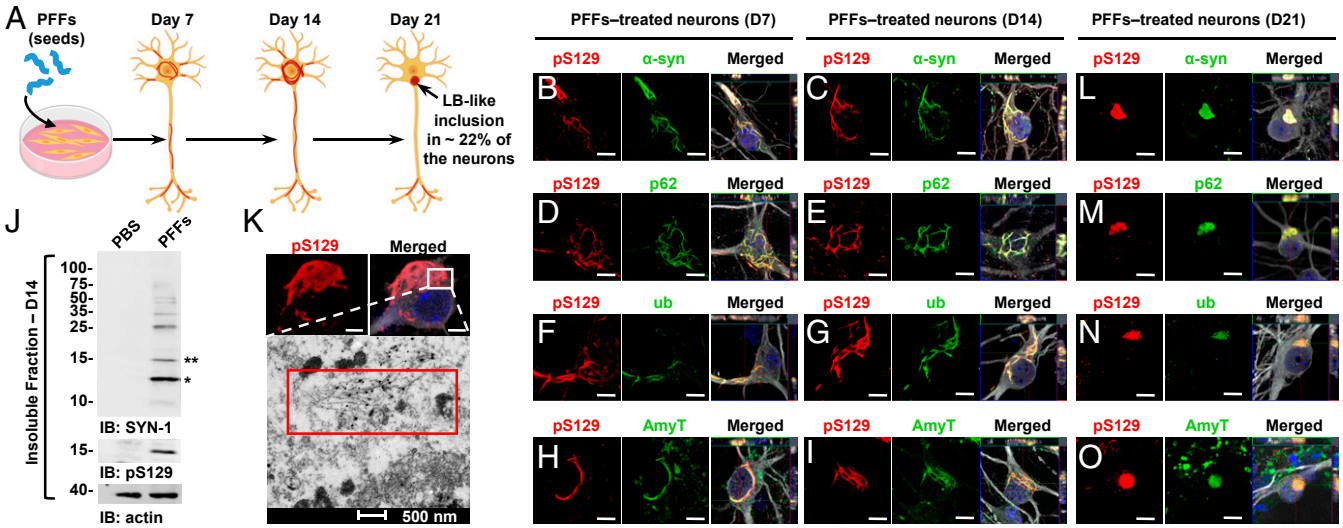

Fig. 1. At early stage, α-syn–seeded fibrillar aggregates share the immunohistochemical but not the structural and morphological features of the bona fide human LBs. (*A*) Seeding model in primary hippocampal neurons. (*B–I* and *L–O*) Temporal analysis of α-syn aggregates formed at D7 (*B*, *D*, *F*, and *H*), at D14 (*C*, *E*, *G*, and *I*), and at D21 (*L–O*) in PFF-treated neurons. Aggregates were detected by ICC using either pS129 (81a) in combination with total α-syn (epitope: 1–20) (*B*, *C*, and *L*) or with the Amytracker dye (AmyT; *H*, *I*, and *O*) or pS129 (MJFR13) in combination with p62 (*D*, *E*, and *M*) or ubiquitin (*F*, *G*, and *N*) antibodies. Neurons were counterstained with MAP2 antibody and the nucleus with DAPI staining. (*J*) Western blot analysis. Total α-syn, pS129, and actin were detected by SYN-1, pS129 (MJFR13), and actin antibodies, respectively. Monomeric α-syn (15 kDa) is indicated by a double asterisk; C-terminal truncated α-syn (12 kDa) is indicated by a single asterisk; the higher molecular weights corresponding to the newly formed fibrils are detected from 25 kDa to the top of the gel. (*K*) At D14, pS129-positive aggregates imaged by confocal microscopy was then examined by EM after immunogold labeling. (Scale bars: *B–I* and *L–O*, 10 μm; *K*, *Upper*, 5 μm.)

formed in the neuronal extensions (D4) are transported over time (D7 to D21) to the perinuclear region, where they eventually accumulate as LB-like inclusions (D21).

The Process of Inclusion Formation Is Accompanied by the Sequestration of Lipids, Organelles, and Endomembranes Structures. The transition from filamentous aggregates into ribbon and round-like aggregates suggests that the newly formed fibrils undergo major structural changes over time. To determine if these changes are associated with the evolution and maturation of α-syn fibrils into LBs, the ultrastructural properties of the seeded α-syn aggregates formed in neurons after 7, 14, or 21 d posttreatment with WT PFFs were characterized using CLEM. In Fig. 2, the CLEM data revealed a marked reorganization of the newly formed α-syn fibrils over time. Indeed, at D7, EM images of neurites positive for pS129^{+} α-syn–seeded aggregates showed predominantly single fibril filaments distant from each other (Fig. 2 *A*, *a*). Aligned and randomly ordered fibrils were observed in the same neurite (Fig. 2 *A*, *a*). In comparison, in neurites negative for α-syn–seeded aggregates, we observed the classic organization of the microtubules that appear as aligned bundle of long filaments parallel to the axis of the neurites (Fig. 2 *A*, *b*). The diameters of the filament-like structures observed in neurites confirmed that the newly formed α-syn fibrils exhibited average diameter of 12 nm, which was significantly smaller than the average diameter of the microtubules (18 nm) (Fig. 2 *A*, *c*). The range of fibril lengths (from 500 nm to 2 μM per slide section) (Fig. 2*A* and *SI Appendix*, Fig. S5 *G–J*) confirmed that the fibrils detected in the cytosol were not simply internalized α-syn PFFs (size ∼40 to 120 nm) (*SI Appendix*, Fig. S5*B*), but rather newly formed fibrils resulting from the seeding and fibrillization of endogenous α-syn. At D7, most of the newly formed α-syn fibrils were observed in neurites and only few in the cell bodies (Fig. 1 *B*, *D*, *F*, *H*). CLEM showed, in the same neuronal cell body, α-syn fibrils randomly organized (Fig. 2 *B* and *C*, blue arrowheads) or ordered as long tracks of parallel bundles of filaments (Fig. 2 *B* and *C*, red arrowheads). At D14, most α-syn filaments were reorganized into laterally associated and tightly packed bundles of fibrils (Fig. 2 *D* and *E*, red arrowheads). In some inclusions, these laterally associated fibrils were seen to start to interact with or encircle organelles, including mitochondria, autophagosomes, and others endolysosomal-like vesicles (Fig. 2 *D* and *E*). Single fibrils, loosely distributed in the neuronal cell body, were also detected close to these organelles.

The sequestration of organelles and membranous structures by α-syn fibrillar aggregates seems to gradually increase over time between D14 and D21 (Fig. 2 *D–F* and *SI Appendix*, Fig. S5*F*). At D21, both the ribbon-like aggregates (Fig. 3 *A* and *B* and *SI Appendix*, Fig. S6*A*, in red) and the LB-like inclusions (Figs. 2*F* and 3 *C* and *D* and *SI Appendix*, Figs. S5*F* and S6*B*, in red) were composed of α-syn filaments (*SI Appendix*, Fig. S6, in black) but also of mitochondria (*SI Appendix*, Figs. S5*F* and S6 *A–D*, in green) and several types of vesicles (Figs. 2*F* and 3 *A–D*), such as autophagosomes, endosome, and lysosome-like vesicles (respectively colored in yellow, pink, and purple in *SI Appendix*, Figs. S5*F* and S6 *A–D*). Higher-magnification images of these organelles are shown in *SI Appendix*, Fig. S6*E*. Interestingly, the mitochondria were either sequestered inside the inclusions or organized at the periphery of the inclusions. The presence of these organelles inside the LB-like inclusions was confirmed by ICC using specific markers for the late endosomes/lysosomes (Fig. 3*E* and *SI Appendix*, Fig. S6*F*) (LAMP1), the mitochondria (Fig. 3*G* and *SI Appendix*, Fig. S6*H*) (Tom20), and the autophagosome vesicles (p62 [Fig. 1*M*] and LAMP2A [Fig. 3*F* and *SI Appendix*, Fig. S6*G*]). BiP, a protein localized to the endoplasmic reticulum (ER), was also partially colocalizing to the LB-like inclusions (Fig. 3*H* and *SI Appendix*, Fig. S6*I*). Our data strongly suggest that the process of inclusion formation is not only driven by the mechanical assembly of newly formed α-syn fibrils, but also seems to involve the sequestration or the active recruitment of other proteins, membranous structures, and organelles over time. This is in line with previous studies showing that LBs from PD brains are not only composed of α-syn filaments and proteinaceous material (34, 41, 42) but also contain a mixture of vesicles, mitochondria, and other organelles (5, 13–15, 43, 44) as well as lipids (23, 24).

The lateral association of the newly formed fibrils at D14 might represent an early stage in the process of packaging fibrillar

Downloaded at Palestinian Territory, occupied on December 1, 2021
www.manaraa.com

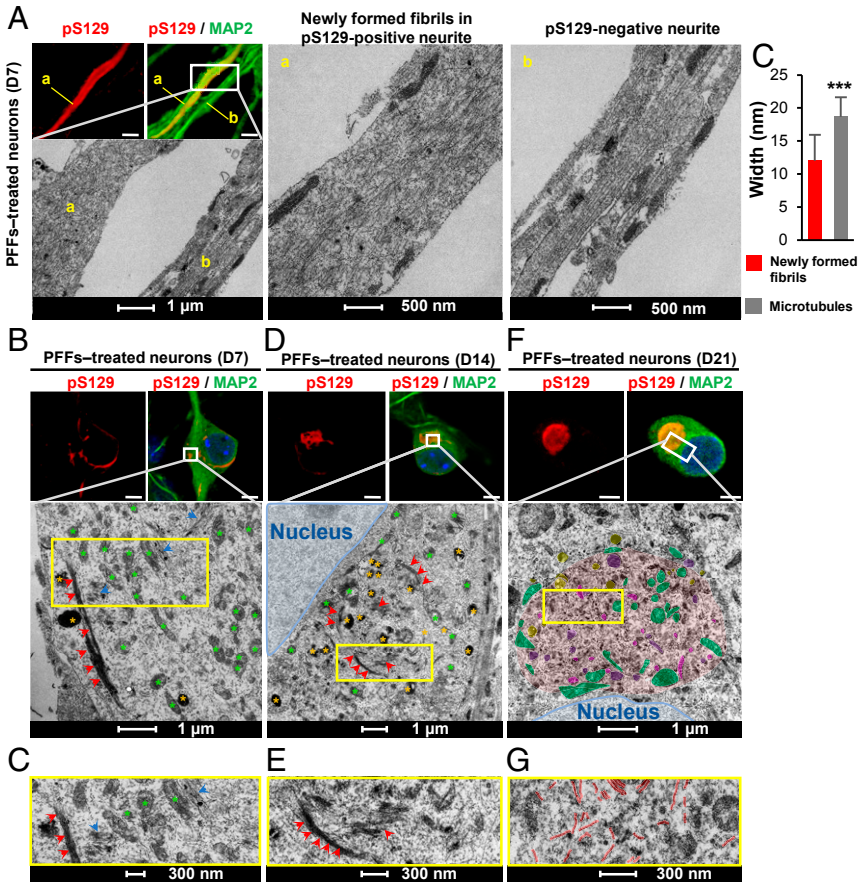

Fig. 2. The formation and maturation of LB-like inclusions require the lateral association and the fragmentation of the newly formed α-syn fibrils over time. At the indicated time, PFF-treated neurons were fixed, ICC against pS129-α-syn was performed and imaged by confocal microscopy (*A*, *B*, *D*, and *F*, *Top*), and the selected neurons were then examined by EM (*A*, *B*, *D*, and *F*, *Bottom*). (*A*, *a*) Neurite with pS129-positive newly formed α-syn fibrils. (*A*, *b*) A neurite negative for pS129 staining. (*A*, *c*) Graph representing the mean ± SD of the width of the microtubules compared to the newly formed fibrils at D7. $^{**}P < 0.001$ (Student's *t* test for unpaired data with equal variance), indicating that this parameter can be used to discriminate the newly formed fibrils from the cytoskeletal proteins. (Scale bars: *A*, *B*, *D*, and *F*, *Top*, 10 μm.) (*C*–*G*) Representative images at higher magnifications corresponding to the area indicated by a yellow rectangle in EM images shown in *B*, *D*, and *F*.

aggregates into LB-like inclusions (25). In addition, the length of the newly formed fibrils significantly decreased over time during the evolution of the inclusions (*SI Appendix*, Fig. S5 *G*–*J*). While at D7 the neurites contained long filaments of α-syn reaching up to 2 μm in length, at D14 the size of α-syn fibrils was significantly reduced to an average length of 400 nm (Fig. 2 and *SI Appendix*, Fig. S5 *G*, *H*, and *J*). This was even more obvious in the compact inclusions observed in neurons treated for 21 d, in which only very short filaments were detected with an average size of 300 nm (Fig. 2 *F* and *G* and *SI Appendix*, Fig. S5 *F*, *I*, and *J*). This suggests that the lateral association of the newly formed fibrils and their packing into higher-organized aggregates might require fragmentation of α-syn into shorter filaments. This is in line with our recent findings showing that specific postfibrillization C-terminal cleavages play important roles in the processing of α-syn seeds and the growth of newly formed α-syn fibrils in the neuronal seeding model (25).

Quantitative Proteomics Reveals the Temporal Sequestration of Membranous Organelle, Synaptic, and Mitochondrial Proteins into LB-Like Inclusions. To gain further insight into the molecular interactions and mechanisms that govern LB formation and maturation, we performed quantitative proteomic analysis on the insoluble fractions of PBS or PFF-treated neurons overtime (Fig. 4 and *SI Appendix*, Fig. S8).

At D7, only α-syn and the phospholipase C β1 (Plcb1) were shown to be significantly enriched in the insoluble fraction with a nine- and twofold increase in the insoluble fraction of the PFF-treated neurons, respectively (*SI Appendix*, Fig. S8*A*). No proteins from the endomembrane compartments were significantly enriched in the insoluble fraction of the PFF-treated neurons at D7. This finding is in line with our CLEM observations showing that at an early stage, α-syn–seeded aggregates were mainly detected in the neurites as long filaments that did not appear to interact with intracellular organelles.

Next, we examined the protein contents of the α-syn inclusions at the intermediate stage, prior to (D14) and after (D21) the formation of LB-like inclusions (Fig. 4). The volcano plots in Fig. 4*A* show that 633 proteins and 568 proteins were significantly up-regulated in the insoluble fraction of the PFF-treated neurons at D14 and D21, respectively (Dataset S1). Classifications of the proteins by cellular compartment (*SI Appendix*, Fig. S8*B*) showed a high enrichment of proteins that belong to the endomembrane compartments mainly from the mitochondria, the ER), the Golgi, and to a lesser extent the endolysosomal apparatus or synapses. These data are in line with the CLEM imaging showing that from D14 the newly formed fibrils start to interact with and encircled several organelles, including mitochondria, autophagosome, endosomes, lysosomes-like vesicles, and other endomembranous structures (Fig. 2*D*) that are found later to be sequestered in the LB-like inclusions at D21 (Figs. 2*F* and 3). Several cytoskeletal proteins, including microtubule and myosin complexes, were also significantly enriched in the insoluble fraction of the PFF-treated neurons (*SI Appendix*, Fig. S8*B*). The close resemblance between the protein contents of the insoluble fraction of PFF-treated neurons at D14 and D21 is expected given

Downloaded at Palestinian Territory, occupied on December 1, 2021
www.manaraa.com

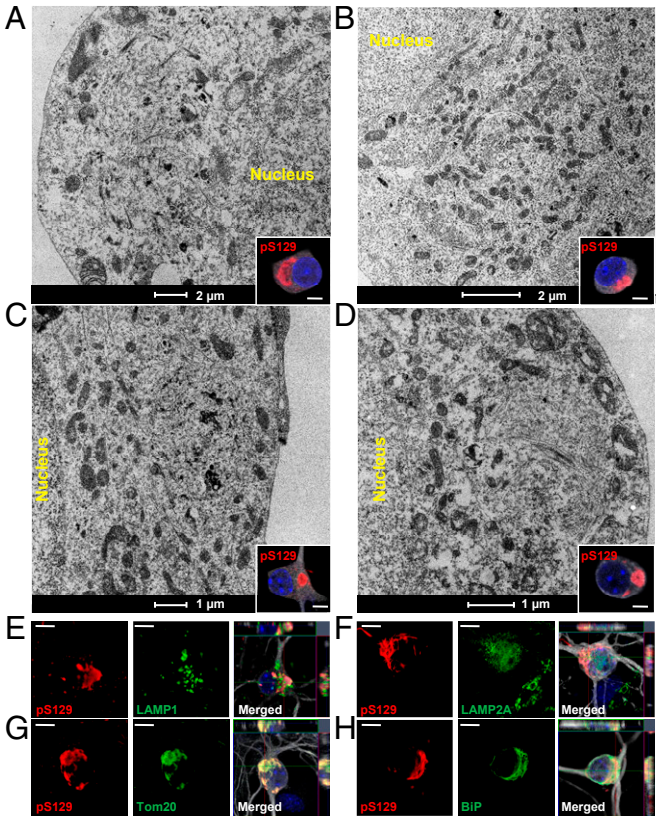

Fig. 3. Maturation of α-syn–seeded aggregates into LB-like inclusions is accompanied by the sequestration of organelles and the endomembrane system. (*A–D*) At D21, PFF-treated neurons were fixed, ICC against pS129-α-syn was performed and imaged by confocal microscopy (*Insets*) and selected neurons were examined by EM. Representative images of LB-like inclusions exhibiting a ribbon-like morphology (*A* and *B*) or compact and rounded structures (*C* and *D*). Mitochondria, autophagosomes, endosome, and lysosome-like vesicles were detected inside or at the edge of these inclusions (see also Fig. S6 *A–E*). (*E–H*) LB-like inclusions were stained by pS129 in combination with organelles markers LAMP1 (late endosomes) (*E*), LAMP2A (autophagosomes) (*F*), Tom20 (mitochondria) (*G*), or BiP (ER) (*H*). Neurons were counterstained with MAP2 antibody and nucleus with DAPI (see also Fig. S6 *F–I*). (Scale bars: *A–D*, *Insets*, 5 µm; *E–H*, 10 µm.)

that at D21 only ∼22% of the positive α-syn aggregates have completely transitioned to inclusions with an LB-like morphology (*SI Appendix*, Fig. S3*E*).

Formation and Maturation of LB-Like Inclusions Are Dynamic Processes, Which Involve Protein Sequestration and Alterations of Key Signaling Pathways Rather than Simply α-Syn Fibrillization. To elucidate the mechanisms and pathways involved in α-syn fibrillization and LB formation and maturation, the proteins enriched in the insoluble fraction of the PFF-treated neurons (Fig. 4*A*) were further classified by biological processes (*SI Appendix*, Fig. S8*C*) and signaling pathways (*SI Appendix*, Fig. S8*D*). At D7 no biological processes were altered (*SI Appendix*, Fig. S8*A*). At D14 and D21, a large number of cytoskeletal proteins, including several tubulin subunits, microtubuleassociated proteins, and motor proteins (kinesin, dynein, and myosin), were detected (*SI Appendix*, Fig. S8 *B* and *C*). This cluster of proteins was associated with the enrichment of several biological processes, including actin cytoskeleton organization, axonogenesis, and dendritic spine development (*SI Appendix*, Fig. S8*C*). The top canonical signaling pathways were also related to axonal guidance and microtubule regulation by the stathmin proteins (*SI Appendix*, Fig. S8*D*). The accumulation of the cytoskeletal proteins in the insoluble fraction was concomitant with the redistribution of newly formed α-syn aggregates from the neurites to the perinuclear region (Fig. 1 *B–O* and *SI Appendix*, Fig. S3 *B–H*). This suggests that the retrograde trafficking of newly formed α-syn fibrils is accompanied by the sequestration of the proteins involved in axonal transport. In line with this hypothesis, our temporal proteomic analysis revealed that, at D14 and D21, the most highly enriched terms for the biological processes were related to intracellular protein transport, including ER to Golgi-mediated transport, the vesicle-mediated transport, and the nucleocytoplasmic protein transport (SI Appendix, Fig. S8 *B* and *C*). Overall, the sequestration of proteins related to the intracellular transport inside α-syn inclusions seems to result in an impairment in the trafficking of organelles and vesicles, such as mitochondria, endosomes, lysosomes, and the synaptic vesicles (45), that eventually accumulate inside α-syn inclusions as evidenced by CLEM imaging (Figs. 2 and 3). In line with this hypothesis, our proteomic data showed perturbation of the biological processes and signaling pathways related to mitochondria and synaptic compartments (Fig. 4*B* and *SI Appendix*, Fig. S8 *C*, *D*, and *F*). Interestingly, not only proteins involved in mitochondrial transport were enriched in the insoluble fraction of the PFF-treated neurons but also proteins related to mitochondrial dynamics, the mitochondrial apoptotic pathway, and the energy metabolism pathways (tricarboxylic acid cycle, ATP, and NADH metabolisms). This indicates that the process of inclusion formation that occurs throughout D14 to D21 might dramatically alter mitochondrial physiology, suggesting that mitochondrial dysfunction could be a major contributor to neurodegeneration in PD and synucleinopathies.

The up-regulation of biological processes related to synaptic homeostasis (*SI Appendix*, Fig. S8 *C* and *F*) was due to the accumulation of both pre- and postsynaptic proteins (*SI Appendix*, Fig. S8 *C* and *F*), mostly at D21 (Fig. 4 *B*, *Right*). The processes involved in synaptic transmission, synapse assembly, and synapse maturation (*SI Appendix*, Fig. S8*C*) were associated with an up-regulation of the long-term synaptic depression and potentiation pathways but also of the endocannabinoid and CXCR4 signaling that regulate synapse function (46) (*SI Appendix*, Fig. S8*D*). Several signaling pathways related to neurotoxicity were also up-regulated in our analyses at D14, such as the Huntington's disease signaling, mitochondrial dysfunction, apoptosis signaling, the ER stress pathway, autophagy, and the neuroinflammation signaling pathway (*SI Appendix*, Fig. S8*D*).

Our proteomic and CLEM data provide strong evidence that formation of LBs does not occur through simply the continued formation, growth, and assembly of α-syn fibrils but instead arises as a result of complex α-syn aggregation-dependent events that involve the active recruitment and sequestration of proteins and organelles over time. This process, which occurs mainly between 14 and 21 d, rather than simply fibril formation, which occurs as early as 7 d, seems to trigger a cascade of cellular processes, including changes in the physiological properties of the mitochondria and the synapses, that could ultimately lead to neuronal dysfunctions and toxicity.

Next, to better understand the mechanisms of dysfunctions that ultimately lead to neurodegeneration, we investigated by RNA-sequencing technology the transcriptomic changes in response to PFFs treatment over time (Fig. 5 and *SI Appendix*, Fig. S9*A* and Dataset S2).

At D7, the differentially expressed genes encoded for proteins located at the synapses, in the axons, or in the secretory and exocytic vesicles (*SI Appendix*, Fig. S9*B*). These genes are thought to play regulatory roles in the neurogenesis processes, including the organization, the growth, and the extension of the axons and dendrites (*SI Appendix*, Fig. S9*C*). Thus, the presence of the newly formed fibrils that are mainly detected in the neuritic extensions at this stage could perturb the development and the differentiation of the neurites. At D14, 329 genes (106 up-regulated, 223 down-regulated) were linked to the synaptic (Fig. 5*A*), neuritic, and vesicular cellular compartments (*SI Appendix*, Fig. S9*B*). These genes were associated with multiple biological processes, including neurogenesis, calcium homeostasis, synaptic

NEUROSCIENCE

Downloaded at Palestinian Territory, occupied on December 1, 2021
www.manaraa.com

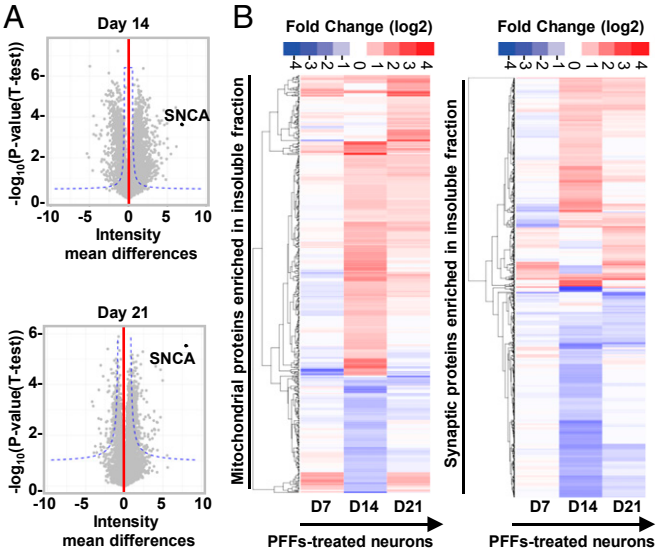

Fig. 4. Temporal proteomic analyses of the protein contents found in the insoluble fraction of the PFF-treated neurons reveals a high increase in proteins related to the endomembrane system. (*A*) Insoluble proteins from neurons treated with PBS and PFFs for 7, 14, and 21 d were extracted and analyzed using LC-MS/MS. Identified proteins were plotted using volcano plot. Dotted lines represent the false discovery rate < 0.05 and threshold of significance SO = 1 assigned for the subsequent analysis. A detailed list of the hits is available in Dataset S1. Classifications of the proteins significantly enriched in the insoluble fractions of the PFF-treated neurons at D14 and D21 by cellular component and biological processes using gene ontology (GO) and DAVID enrichment analyses are shown in *SI Appendix*, Fig. S8 *B* and *C*. (*B*) Heat maps representing color-coded fold-change levels of mitochondrial (*Left*) and synaptic (*Right*) proteins present in the insoluble fraction in PFF-treated neurons.

homeostasis (organization, plasticity, and neurotransmission), cytoskeleton organization, response to stress, and neuronal cell death process (*SI Appendix*, Fig. S9*C*).

At D21, our transcriptomic data showed an enrichment of genes that encode for proteins related to the ion channel complex, plasma membrane protein complex, and the cell–cell junctions. More importantly, our data show that the expression level of 217 synaptic related genes was dramatically changed over time with a marked difference between D14 and D21 (Fig. 5*A* and *SI Appendix*, Fig. S9 *B*–*D*). Strikingly, at D21, ~20% of the genes differentially expressed in the PFF-treated neurons were related to synaptic functions, including neurotransmission processes and synapse organization. Also, at D21, biological processes related to the response to oxidative stress and mitochondria, including mitochondrial disassembly, mitophagy, and mitochondrial depolarization, were significantly enriched (Fig. 5*B*).

Altogether, our results show that alterations of the mitochondrial and synaptic functions, both at the proteomic and transcriptomic levels, occur primarily throughout D14 to D21, thus coinciding with inclusion formation, LB maturation, and cell death.

Dynamics of LB Formation and Maturation Induce Mitochondrial Alterations. To validate our findings that mitochondrial dysfunctions are associated with the formation of the LB-like inclusions, we assessed the mitochondrial activity over time in PFF-treated neurons. ICC for mitochondrial markers (VDAC1, TOM20, and TIM23) revealed strong colocalization of mitochondria with α-syn pS129$^+$ aggregates starting from D14 after PFF exposure (*SI Appendix*, Fig. S10*A*). To assess whether this recruitment of mitochondrial components influences mitochondrial function, we applied a combined protocol of high-resolution respirometry with Amplex red-based fluorometry to measure the production of mitochondrial reactive oxygen species (ROS). Routine respiration of intact cells was significantly reduced at D21 (Fig. 6*A*), while it was similar to PBS-treated control cells at the other assessed time points (D7 and D14). Plasma membranes were subsequently permeabilized using digitonin, and substrates feeding into NADH-linked respiration were supplied. In the absence (N_L) and presence (N_P) of ADP, these respirational states did not significantly differ across all tested time points following PFF and PBS treatment.

Addition of succinate drove overall respiration of all other groups to significantly higher levels than neurons at D21. This was the case for both maximum oxidative phosphorylation capacity (NS_P) and maximum electron transport system capacity (NS_E) in the uncoupled state (by carbonyl cyanide m-chlorophenyl hydrazine [CCCP]). Blocking NADH-linked respiration by rotenone, yielding maximal succinate-driven respiration in the CCCP uncoupled state, maintained the significantly lower respiration of neurons at D21. Strikingly, the generation of mitochondrial ROS was significantly decreased at D7 but returned to baseline levels after longer periods of PFF treatment (Fig. 6 *A*, *Lower*). In line with respiration results, analysis of proteomic data revealed significant recruitment of oxidative phosphorylation system components into aggregates starting from D14 (Fig. 6*C*). Complexes I, II, and V were strongly affected up to D21, with complex II subunit SDHC being robustly detected in aggregates at D14 and D21 (Fig. 6 *B* and *F*). The strong sequestration of complex II components into aggregates might explain the stronger effects of α-syn pathology on succinate- than on NADH-linked substrate-driven respiration.

The reduced mitochondrial ROS production at D7 (Fig. 6*A*) correlated with the apparent lack of mitochondrial proteins involved in oxidative stress responses in α-syn aggregates (*SI Appendix*, Fig. S8 and Dataset S2). Coinciding with the appearance of proteins and components of the JNK pathway in the α-syn aggregates (*SI Appendix*, Fig. S8 and Dataset S2), mitochondrial ROS production

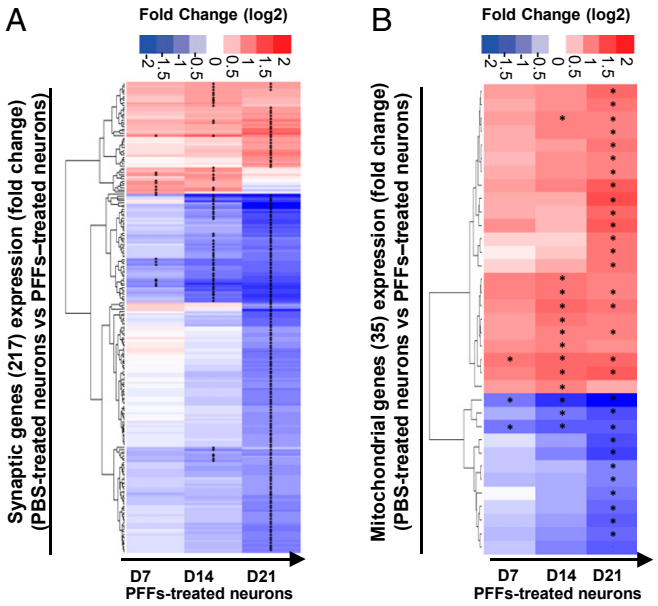

Fig. 5. Gene-expression level changes during the formation of the newly formed fibrils and their maturation into LB-like inclusions. Temporal transcriptomic analysis of the gene-expression level in PBS-treated neurons vs. PFF-treated neurons treated for 7, 14, or 21 d. Genes with an absolute log2 fold change greater than 1 and a false discovery rate less than 0.01 were considered as significantly differentially expressed (*SI Appendix*, Fig. S9). Dataset S2 depicts the number of genes up- or down-regulated in PFF-treated neurons over time. (*A* and *B*) Log2 fold changes of the mitochondrial genes (*A* and Dataset S3), and the synaptic genes (*B* and Dataset S4) expression levels are represented over time. "*" indicates a significant up- or down-regulation in the gene-expression level.

Downloaded at Palestinian Territory, occupied on December 1, 2021
www.manaraa.com

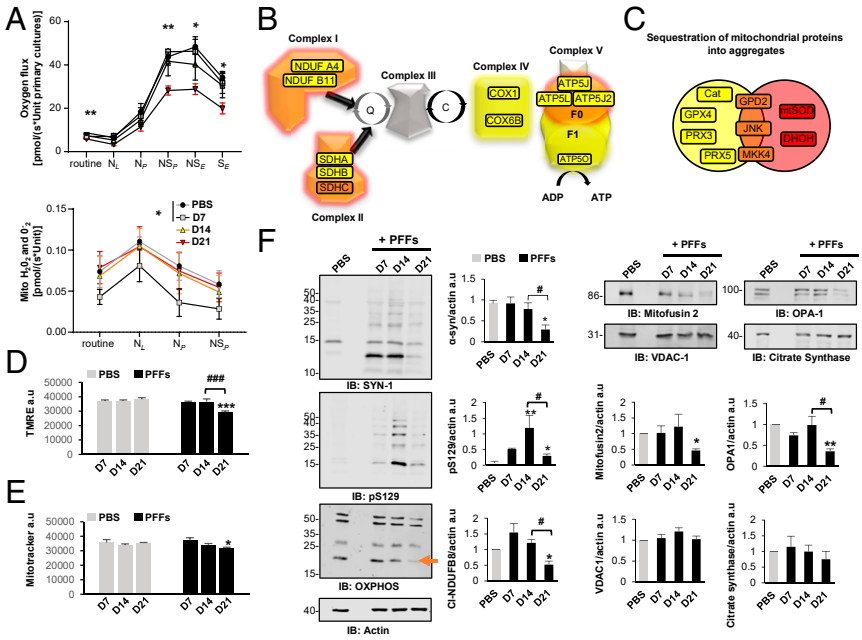

Fig. 6. Dynamics of Lewy body formation and maturation induce mitochondrial alterations. (*A*) High-resolution respirometry measurements. Statistical results were obtained from two-way repeated measurement ANOVAs based on a minimum of four independent experiments. (*B* and *C*) Proteomic data on proteins implicated in mitochondrial dysfunction. (*D*) Mitochondrial membrane potential was assessed fluorometrically from cells loaded with TMRE. (*E*) Measurement of mitotracker green level, which labels mitochondrial proteins independently of mitochondrial membrane potential. (*F*) Western blot analyses of total fractions immunoblotted with antibodies against components of the OXPHOS complexes I-V, mitofusin 2, OPA1, citrate synthase, and VDAC1 proteins. Actin was used as the loading control. The graphs (*D–F*), represent the mean ± SD of a minimum of three independent experiments. $^{*}P < 0.05$, $^{**}P < 0.005$, $^{***}P < 0.0005$ (ANOVA followed by Tukey honest significant difference [HSD] post hoc test, PBS- vs. PFF-treated neurons). $^{\#}P < 0.05$, $^{\#\#\#}P < 0.0005$ (D14 vs. D21 PFF-treated neurons). a.u., arbitrary unit.

increased to baseline levels. Mitochondrial membrane potential was measured from attached cells by tetramethylrhodamine, ethyl ester (TMRE) fluorometry (Fig. 6*D*), and in line with respiration data, deterioration of mitochondrial membrane potential was apparent only at D21. At this time point, we also observed a slight reduction of membrane potential-independent binding of Mitotracker green to mitochondrial proteins (Fig. 6*E*), indicating moderate loss of mitochondrial density.

To investigate the effects of the aggregation process on mitochondrial proteins in more detail, Western blot analyses were performed and the expression levels of outer mitochondrial membrane proteins (mitofusin 2 and VDAC1), matrix protein (citrate synthase), inner mitochondrial membrane proteins, including OPA1 and subunits of oxidative phosphorylation complexes (OXPHOS), known to be labile when the respective complexes are not assembled, were measured overtime. At D7 and D14, no altered mitochondrial protein levels were observed despite reduced mitochondrial ROS production and increases in α-syn pS129 and HMW species (Fig. 6*F* and *SI Appendix*, Fig. S11*C*). Significant reductions were only observed at D21 for profusion protein OPA1 (long and short isoforms) and mitofusin 2 (Fig. 6*F* and *SI Appendix*, Fig. S11*C*). Similar effects were observed for subunits of OXPHOS, in particular complex I subunit NDUFB8 (Fig. 6*F* and *SI Appendix*, Fig. S11*C*). Importantly, levels of VDAC1 and citrate synthase, common markers of mitochondrial density, remained relatively unaffected, even in this period of massive respirational deficits and dropping mitochondrial membrane potential.

Synaptic Dysfunction Is Primarily Linked to the Formation and the Maturation of the LB-Like Inclusions. Our transcriptomic and proteomic data strongly suggest that the reorganization of the newly formed fibrils into LB-like inclusions appeared to be associated with synaptic alterations (Figs. 4*B* and 5*A*). Therefore, we assessed by Western blot analysis the protein levels of pre- and postsynaptic markers (synapsin I, postsynaptic density 95 [PSD95]). We measured a dramatic reduction of these synaptic markers at D21 both in the primary neuronal culture (Fig. 7*A*) or specifically in the neuronal population (*SI Appendix*, Fig. S11*D*). ICC analysis of synapsin I (Fig. 7*B*), VAMP2, and SNAP2 (*SI Appendix*, Fig. S12 *A* and *B*) staining confirmed the significant loss of synapses in neurons containing inclusions from D21 (Fig. 7*C*). This finding correlates with the marked increase in neuronal cell death observed at D21 (*SI Appendix*, Fig. S14 *A–K*). Finally, both proteomic and transcriptomic data suggested dysregulation of the mitogen-activated protein kinase (MAPK) signaling pathways and the recruitment of the MAPKs ERK1 (MAPK3) and ERK2 (MAPK1) within α-syn inclusions over time, as the ERK signaling pathway is involved in regulating mitochondria fission and integrity (47) and synaptic plasticity (48, 49), and is also an important player in PD pathogenesis (50, 51). Western blot analysis showed a significant reduction of the total protein level of the extracellular signal-regulated (ERK 1/2) proteins, with the remaining protein being highly phosphorylated at D21. Finally, ICC revealed that p-ERK 1/2 decorated the newly formed fibrils at D14 before being sequestered in the LB-like inclusions at D21 (*SI Appendix*, Fig. S12*C*). In addition, our data showed that p-ERK 1/2 was only associated with the newly formed aggregates localized in the neuronal cell bodies, as evidenced by the absence of p-ERK 1/2 signal near the neuritic aggregates at D7 and D14. At D21, the granular p-ERK 1/2 immunoreactivity was mostly detected at the periphery of the inclusions as observed in the bona fide LBs found in human PD brain tissue (52, 53).

The Formation and Maturation of the LB-Like Inclusions Are Associated with Neuronal Cell Death. We next assessed how the processes of formation of α-syn aggregates and their maturation into LB-like inclusions impact on the health of the cells over time.

First, treatment of α-syn KO neurons with α-syn PFFs did not induce neuronal death, confirming that α-syn PFFs uptake is not toxic (*SI Appendix*, Fig. S13). Cell death was detectable in WT neurons treated with PFFs but not with PBS (*SI Appendix*, Fig. S14 *A–G*), starting from D14 as evidenced by the activation of caspase 3 (*SI Appendix*, Fig. S17*D*). The loss of plasma membrane integrity was observed starting at D19, as reflected by the release of lactate dehydrogenase (LDH) that significantly increased at D21 (*SI Appendix*, Fig. S14 *B* and *C*). Terminal dUTP nick end-labeling (TUNEL) assay combined with NeuN (a specific neuronal marker) and pS129 staining showed that the glial cells ($TUNEL^{+}$ $NeuN^{-}$) were the most affected in the PFF-treated primary culture up to D14, (*SI Appendix*, Fig. S14 *E* and *F*), whereas neuronal loss ($TUNEL^{+}/NeuN^{+}$) was only significantly observed at D21 (*SI Appendix*, Fig. S14 *E–G*). Moreover, the neurons containing seeded aggregates exhibited more cell death

NEUROSCIENCE

Downloaded at Palestinian Territory, occupied on December 1, 2021
www.manaraa.com

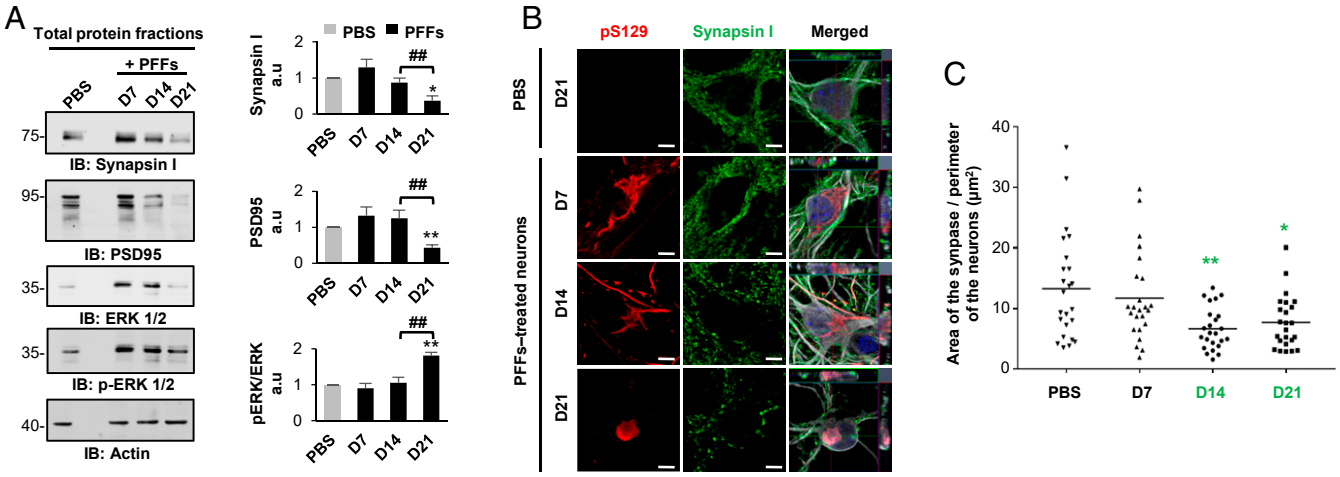

Fig. 7. Synaptic dysfunctions were associated with the formation and maturation of the LB-like inclusions. (*A*) The levels of Synapsin I, PSD95, and ERK 1/2 were assessed by Western blot over time. Actin was used as the loading control. The graphs represent the mean ± SD of a minimum of three independent experiments. (*B* and *C*) Synaptic area decreases in PFF-treated neurons from D14. (*B*) Aggregates were detected by ICC using pS129 (MJFR13) and Synapsin I antibodies. Neurons were counterstained with MAP2 antibody, and the nucleus with DAPI. (Scale bars: 5 µm.) (*C*) Measurement of the synaptic area was performed over time. (*A* and *C*) ANOVA followed by Tukey honest significant difference [HSD] post hoc test was performed. $^{*}P < 0.05$, $^{**}P < 0.005$ (PBS- vs. PFF-treated neurons). $^{\#\#}P < 0.005$ (D14 vs. D21 PFF-treated neurons). a.u., arbitrary unit.

than the neurons without aggregates (*SI Appendix*, Fig. S14*H*). Our findings suggest that despite the major cellular dysfunctions induced by the formation of the LB-like inclusions, only a slow and progressive cell death response was observed in the neurons.

Strikingly, our transcriptomic analysis revealed that 156 genes involved in signaling pathways related to the regulation of neuronal cell death were also significantly changed over time in PFF-treated neurons (*SI Appendix*, Fig. S14 *L* and *M*). These genes started to be significantly dysregulated at D14. At D21, 70 genes involved in cell death signaling pathways were up-regulated in PFF-treated neurons compared to PBS-treated neurons (*SI Appendix*, Fig. S14*L*). Among these genes, 24 were directly related to apoptotic pathways, which is in line with our cell death assays showing significant activation of caspase 3 at D21. Between D14 and D21, 26 genes were differentially expressed in PFF-treated neurons (*SI Appendix*, Fig. S14*M*).

Our data also revealed a significant reduction of α-syn mRNA levels at D21 (*SI Appendix*, Fig. S14*N*), concomitant with the down-regulation of the transcript level of the Polo-like kinase 2 (Plk2) (*SI Appendix*, Fig. S14*O*), one of the main kinases involved in the phosphorylation of α-syn at S129 residue. This suggests that several cellular responses are deployed by the neurons to prevent further aggregation and inclusion formation, either by down-regulation of the protein level of α-syn or its phosphorylation state. Overall, our data suggest a progressive neurodegeneration that coincides with the first signs of organelle accumulation and assembly of the LB-like inclusions.

Discussion

The Majority of Existing Cellular Models Are Models of α-Syn Fibril Formation Rather than LBs. Several in vitro assays (54–57) and cellular and animal models (9, 10, 21, 22, 44, 55) of α-syn aggregation and pathology formation have been developed and are commonly used to study these processes. While many of these models reproduce specific aspects or stages of LB pathology formation, none has been shown to form pathological aggregates exhibiting the biochemical and organizational complexity of α-syn pathologies, including LBs, found in postmortem brains of patients with synucleinopathies (5, 13–15, 23, 24, 31, 43, 44). For the most part, classification of α-syn aggregates as having LB-like features has been limited to very few biomarkers (8–10), namely pS129, ub, and p62 immunoreactivity and the detection of HMW aggregates in Western blotting (8, 21, 32, 33). In very few cases, detailed studies were performed to characterize the nature of the aggregates and their morphological properties (8, 21, 32, 33). Failure of these models to reproduce the transition of α-syn from the aggregated/fibrillar stage to LB-like inclusions has hampered efforts to elucidate the molecular determinants and cellular pathways that regulate the different stages of LB pathology formation and to determine the role of this process in the pathogenesis of PD.

The use of PFFs to seed the aggregation of endogenous α-syn has enabled the reliable induction of α-syn fibril formation in neurons and other cell types (44, 58). Based on the use of the LB markers discussed above, these seeding models are often presented as models of LB pathology. However, EM studies (21, 32, 33) of the seeded aggregates, including our own (Fig. 2 *A*–*F*), clearly show the presence of mainly fibrillar aggregates at the time points usually used to assess seeding in this model (10 to 14 d) (Figs. 1 and 2). These observations demonstrate that the α-syn modifications and interacting proteins commonly used to define LB pathology represent markers of α-syn fibril formation and not necessarily LB pathology, although these markers persist with α-syn fibrils during their transition to LBs and other types of α-syn pathologies.

Extending the Seeding Process Enabled the Reconstitution of LB-Like Inclusions in Neurons. While investigating the mechanism of seeding and pathology spreading in mice inoculated with PFFs, we observed a time-dependent shift in the morphology and localization of α-syn pathology from a filamentous neuritic fibrillar pathology to predominantly compact α-syn in cell body inclusions. Similarly, we observed that by simply extending the seeding process in primary neurons from 14 to 21 d, we began to see major changes in the localization and biochemical properties of the fibrils that eventually led to the formation of rounded LB-like inclusions (Figs. 2*F* and 3 and *SI Appendix*, Fig. S5*F*) that exhibit similar biochemical, structural, and architectural features as patient-derived LBs, as previously described by EM- (4, 5, 14–16, 35, 43, 59), immunohistochemical (IHC)-, or ICC-based imaging (31, 34, 60), Western blot (26–30), and proteomic (41, 42) analyses. This includes the cleavage (25) and accumulation of truncated fibrillar α-syn species (26–30), the presence of many of the proteins found in LBs (34, 41, 42) and the active recruitment of membranous organelles (e.g., mitochondria, the endolysosomal apparatus, and autophagolysosome-like vesicles) (5, 13–15, 23, 24, 31, 36, 43, 44, 59, 61). Although previous reports have established the presence of lipids in LBs from postmortem PD tissues using different

Downloaded at Palestinian Territory, occupied on December 1, 2021
www.manaraa.com

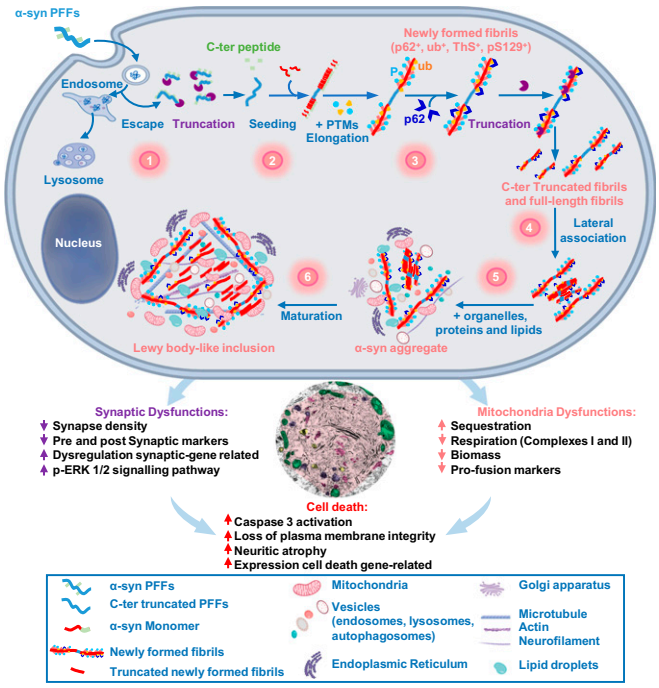

Fig. 8. The dynamics of Lewy body formation, rather than simply α-syn fibrillization, is the primary cause of mitochondrial alterations, synaptic dysfunction, and neurodegeneration. Formation of α-syn inclusions in the context of the neuronal seeding requires a sequence of events starting with 1) the internalization and cleavage of PFF seeds (D0–D1); followed by 2) the initiation of the seeding by the recruitment of endogenous α-syn (D0–D4); 3) fibril elongation along with the incorporation of posttranslational modifications (PTMs), such as phosphorylation at residue S129 and ubiquitination (D4–D14); 4) formation of seeded filamentous aggregates (D7) that are fragmented and laterally associated over time (D7–D21); and 5–6) the packing of the fibrils into LB-like inclusions (D14–D21), which have a morphology similar to the bona fide LB detected in human synucleinopathies (D21), is accompanied by the sequestration of organelles, endomembranes, proteins, and lipids. Our integrated approach using advanced techniques in EM, proteomics, transcriptomics, and biochemistry clearly demonstrate that LB formation and maturation impaired the normal functions and biological processes in PFF-treated neurons, causing mitochondrial alterations and synaptic dysfunctions that result in a progressive neurodegeneration.

techniques, including coherent anti-Stokes Raman scattering microscopy (16, 38) or synchrotron Fourier transform infrared microspectroscopy (39), very few studies have explored the different types of lipids and their distribution in LBs. Using different probes that target different types of lipids, we identified several classes of lipids that colocalize within the LB-like structures. Consistent with our confocal and CLEM imaging data, we observed enrichment of lipids (methyl ester staining) (*SI Appendix*, Fig. S3 *K–P*) that are specific for mitochondria, ER, and Golgi apparatus membranes within the LB-like inclusions. In addition, the phospholipids (cell membranes) (24), sphingolipids (ER and Golgi complex) (24), neutral lipids (23, 24) (lipid droplets), and the cholesteryl esters (24) (cholesterol transport), which have been previously reported as components of the bona fide LB inclusions were also detected, reinforcing the similarities between the LB pathologies in PD and the LB-like inclusions formed in the seeding model. These findings underscore the critical importance of reassessing the role of lipids in the different stages of α-syn aggregation and LB formation and maturation.

Altogether our findings are in agreement with ultrastructure-based studies showing that LBs imaged in the substantia nigra (12, 13, 15, 16, 43, 59), the hippocampal CA2 region (62), or the Stellate ganglion (5) from PD patients or non-PD patients (14) exhibit organized structures that are enriched in deformed and damaged mitochondria, cytoskeletal components, and lipidic structures, including vesicles, fragmented membranes of organelles, and presynaptic structures. In a recent study, Shahmoradian et al. used the CLEM approach to characterize LBs in substantia nigra and showed that all LBs are enriched in membranous organelles and lipids, but not all LBs contained α-syn fibrils (16). However, a stimulated emission depletion microscopy study of similar LBs conducted by the same group revealed the presence of a highly dense and organized shell of phosphorylated α-syn at the periphery of these LBs (38). These observations raise the possibility that the CLEM procedure could have led to the disruption and removal of this peripheral aggregated pS129–α-syn. One alternative explanation that is consistent with our findings in the neuronal model is that the fibrils become increasingly fragmented over time (Fig. 2 and *SI Appendix*, Fig. S5*J*) (~50 to 350 nm in length at D21 in PFF-treated neurons). Such small fibrils, which are also C-terminally truncated (25), might not be recognized or could be missed, especially when C-terminal antibodies were used to identify LBs (pS129 antibody or total α-syn antibody against amino acids 115 to 122) (16). We cannot rule out the possibility that LB structures devoid of fibrillar α-syn aggregates exist and could represent a rare type of α-syn pathologies in PD and synucleinopathies. Indeed, several reports have confirmed the existence of a large morphological spectrum of LBs (6, 14, 31, 35, 43, 63–65).

Altogether, our results suggest that the neuronal seeding model recapitulates many of the key events and processes that govern α-syn seeding, aggregation, and LB formation (Fig. 8 and *SI Appendix*, Fig. S15). This model also allows disentangling of the two processes of fibril formation and LB formation, thus paving the way for systematic investigation of the molecular and cellular determinants of each process and their contributions to neuronal dysfunction and degeneration.

The Proteome of the Neuronal LB-Like Inclusions Overlaps with that of PD and Points to Failure of the Protein Degradation Machinery to Clear α-Syn Inclusions. To further characterize the pathological relevance of the inclusions formed in the neuronal seeding model, we compared our proteomic data with results from previous studies on the proteome of brainstem or cortical LBs from PD human brain tissues. Approximately one-fourth of the proteins identified in our inclusion proteomic data at D14 and D21 were previously described as components of the LBs based on immunohistochemical-based studies (7, 11, 34) (*SI Appendix*, Fig. S8*G*). When comparing our proteomic data of the LB-like inclusions with the proteome of human LBs, we found that ~15 to 20% of the proteome overlaps with that of LBs from human PD brain tissues (41, 42). This is not surprising given the differences in the time of LB inclusion formation and maturation between primary neurons and in the human brain. It is also evident from our CLEM studies that the neuronal LB-like inclusions have not reached the same mature stage as the PD LBs. Interestingly, even previous studies that investigated the protein content of human cortical LBs showed ~20% of similarities in the proteome of the inclusions. Overall, most of the proteins found in common between LBs from PD human brain tissues and the LB-like inclusions from the neuronal seeding model could be classified into three main categories: 1) Proteins from the mitochondria and synaptic compartments or belonging to the endomembrane system; 2) cytoskeleton constituents and proteins associated with the intracellular trafficking of proteins and vesicles and the nucleocytoplasmic transport; and 3) proteins involved in the protein quality control and the degradation/clearance machineries (*SI Appendix*, Figs. S8 *G* and *H*).

These results suggest that the sequestration of proteins related to the intracellular transport inside α-syn inclusions might result in impaired trafficking of organelles and vesicles, such as mitochondria, endosomes, lysosomes, and the synaptic vesicles. Interestingly, dysfunction of the intracellular trafficking system and, in particular defects in the ER/Golgi caused by α-syn, have been shown to underlie the pathogenesis of PD at the early stage (45). Previously published proteomic analyses using the same

NEUROSCIENCE

Downloaded at Palestinian Territory, occupied on December 1, 2021

www.manaraa.com

neuronal seeding model also indicated a potential role of the microtubule-dependent transport of vesicles and organelles (66) during the process of aggregate formation (*SI Appendix*, Fig. S8*E*). Finally, the accumulation of large components of the proteins involved in the protein quality control and degradation/clearance machinery inside LB-like inclusions and the human bona fide LBs point toward a potential failure of the protein degradation machinery to clear off α-syn inclusions, leading to the intracellular accumulation of the aggregates as failed aggresomes-like inclusions. In line with this hypothesis, it has been shown that a conditional KO of 26S proteasome in mice led to the formation of LB-like inclusions composed of filamentous α-syn, mitochondria, and membrane-bound vesicles in neurons (67). This is also consistent with our proteomic results showing a marked enrichment of the proteasomal system between D14 and D21 in the insoluble fractions of the PFFs-treated neurons (Fig. 4 and *SI Appendix*, Fig. S8*H*). Altogether, these findings highlight the potential role of the proteasomal system in the formation of LBs.

The Processes Associated with LB Formation and Maturation, Rather than Simply α-Syn Fibril Formation, Are One of the Major Drivers of α-Syn Toxicity in Neurons. Several studies have suggested that the formation of LBs represents a protective mechanism whereby aggregated and potentially toxic α-syn species are actively recruited into aggresome-like structures to prevent their aberrant interactions with other cytosolic proteins and their deleterious effects on cellular organelles (68). A protective role for LBs is plausible if one assumes that this process is efficient. However, if this process stalls for any reason, then this will likely expose neurons to deleterious effects mediated by the presence of toxic proteins and damaged organelles and vesicles. To test this hypothesis, it is crucial to develop a neuronal and animal model system that enables uncoupling of the different stages of α-syn aggregation, fibrillization, and LB formation. One key advantage of neuronal models, as shown in this study, is that they permit detailed investigation of the molecular and cellular changes that occur during LB formation with high temporal resolution.

Our results show that formation of α-syn fibrils occurs as early as D4 to D7, primarily in neurites, where they accumulate as long filamentous fibrils (Fig. 1 *B*, *D*, *F*, and *H* and 2 *A*, *a*). At the early stage of the seeding and fibrillization process (D7), the presence of these newly formed fibrils did not result in significant alteration of the proteome (Fig. 4 and *SI Appendix*, Fig. S8*A*), and induced only limited genetic and molecular perturbations (Figs. 4 and 5) that did not impact neuronal viability up to D14 (*SI Appendix*, Fig. S14 *A–K*). These findings are in line with previous studies where no cell death was reported before D14 (21, 32, 33, 69, 70) and suggest that α-syn fibrillization is not sufficient to trigger neuron death, despite the large accumulation of α-syn fibrils throughout the cytosol of neurons.

However, the progressive accumulation of the filamentous fibrils in the neuronal cell bodies from D7 to D14 was accompanied by the shortening of the fibrils, their lateral association, and their interaction with surrounding organelles (Fig. 2). These structural changes were concomitant with significant perturbations at the proteomic (Fig. 4) and transcriptomic levels (Fig. 5). Despite the interaction of the newly formed fibrils with a large number of proteins associated with cytoskeleton organization, mitochondrial functions, intracellular trafficking of proteins, vesicles, and nucleocytoplasmic transport, only the early stages of cell death were activated at D14, as evidenced by the significant activation of caspase 3 yet without the loss of plasma membrane integrity (*SI Appendix*, Fig. S14 *A–D*). The enrichment of proteins related to the chaperones machineries, the autophagy-lysosomal pathway, and the ub-proteasome system in the insoluble fraction of the PFF-treated neurons at D14 (*SI Appendix*, Fig. S8 *G* and *H*) could suggest that the engagement of the protein quality control machinery and other related processes represent early cellular responses to prevent the formation or the accumulation of the fibrils in the cytosol. Similarly, transcriptomic analyses revealed that the formation of α-syn–seeded aggregates induced (between D7 and D14) major dysregulations in the expression of genes involved in neurogenesis, calcium and synaptic homeostasis, cytoskeleton organization, response to stress (*SI Appendix*, Fig. S9), and neuronal cell death process (*SI Appendix*, Fig. S14 *L–M*). Therefore, the lack of noticeable toxic effects during the fibrillization process (D7 to D14) might reflect the ability of neurons to activate multiple pathways to counter any negative effects induced by the fibrils.

In our extended neuronal seeding model, we observed that the major changes in the structural properties of the newly formed fibrils occur between D14 and D21. This suggests that alternative cellular mechanisms take over to allow the structural reorganization of the fibrils and their sequestration within LB-like inclusions. This could represent an ideal detoxification mechanism by reducing aberrant interactions of the fibrils with cytosolic proteins or organelles. However, our CLEM (Fig. 3) and proteomic analyses (Fig. 4) showed that these structural changes were accompanied by significant recruitment and aberrant sequestration of intracellular proteins related to the intracellular transport inside α-syn inclusions. This seems to result in the trafficking impairment of organelles and vesicles, such as mitochondria, endosomes, lysosomes, and the synaptic vesicles (45) that eventually accumulate within LB-like inclusions (Figs. 2–4). This process was coupled with altered expression of genes associated with the cytoskeleton, mitochondria, and synaptic pathways together with an increase of the neuronal cell death pathways and neurodegeneration (Figs. 5–8 and *SI Appendix*, Fig. S14). Our data suggest that postfibrillization posttranslational modifications could play important roles in these processes by regulating the interactome of the fibrils and their interactions with cellular organelles. The sequestration of proteins and organelles eventually leads to a widespread loss of their biological functions, ultimately resulting in neurodegeneration. In response, neuronal or organelle dysfunctions, induced by α-syn aggregation could also contribute to driving the process of LB-like inclusion formation. Finally, the reorganization of the newly formed fibrils into LB-like inclusions was accompanied by a significant decrease of α-syn both at the protein (*SI Appendix*, Fig. S7) and mRNA (*SI Appendix*, Fig. S14*N*) levels. While depletion of endogenous α-syn could prevent further aggregation and inclusion formation, it could also lead to loss of important physiological functions of α-syn with cellular dysfunctions as consequences.

The Dynamics of LB Formation and Maturation Induce Mitochondrial Alterations. The prominent accumulation of mitochondria and mitochondrial components within the LB-like inclusions prompted us to further investigate how the various stages of α-syn fibrillization and LB formation influence mitochondrial functions (*SI Appendix*, Fig. S10 *B–D*). Although mitochondrial dysfunctions have been strongly implicated in PD and other neurodegenerative diseases (71, 72), the mechanisms by which mitochondrial dysfunction is induced and how it promotes pathology formation and neurodegeneration are still unclear.

Based on our CLEM results and literature evidence, we propose that interactions between the newly formed α-syn aggregates and mitochondria (D7 to D14) result in the increasing sequestration of mitochondrial organelles and proteins during the formation and the maturation of the LB-like inclusions, leading to severe mitochondria defects at D21 (Figs. 3–6 and *SI Appendix*, Fig. S10 *B–D*). This is in line with proteomic (41, 42), IHC (34), and EM (13, 15, 16, 35, 43) results obtained for LBs in postmortem PD brain tissues, which contain mitochondrial proteins and relatively intact mitochondrial organelles.

Based on our results, we suggest a working model on how subtle mitochondria-related events across the formation and maturation of LB-like inclusions might induce neurodegeneration (*SI Appendix*, Fig. S10 *B–D*).

A reduction in mitochondrial complex I, and of the profusion proteins mitofusin 2 and OPA1 protein levels by Western blot

Downloaded at Palestinian Territory, occupied on December 1, 2021
www.manaraa.com

(Fig. 6) was only observed on D21, indicating an eventual failure of compensatory mechanisms during the formation of LB-like inclusions. These observations correlate with reduced mitochondrial membrane potential and a breakdown of mitochondrial respiration at this time point. Decreased respiration has already been shown in previous studies in the neuronal seeding model. However, respiration was assessed only between 8/9 and 14 d after PFFs treatment using mouse cortical neurons (73) or rat midbrain neurons (74), respectively. Importantly, in these previous studies high PFF concentrations (140 nM or 350 nM) were used, which in our hands induce cell death events faster. The concentration applied here (70 nM) allowed investigation at a state, where LB-like inclusions occur. While mitochondrial respiration in these reports was assessed only in intact cells, here we measured maximum respiratory capacities at states requiring plasma membrane permeabilization. This allowed the additional determination of the contribution of mitochondrial complexes I and II to total mitochondrial respiration capacities. Our data are in line with postmortem studies (75–77) reporting the deficiency of the respiratory chain in substantia nigran eurons from PD patients.

Given that we were able to detect different types of changes in mitochondrial functions and biochemical properties during the different stages associated with α-syn aggregation, fibrillization and formation of LB-like inclusions, we believe that the seeding model provides a powerful platform for dissecting the role of mitochondrial dysfunctions in synucleinopathies.

Synaptic Functions Are Impaired during the Formation and the Maturation of the LB. Several studies on postmortem PD brain tissues and animal models have recently suggested that neuritic and synaptic degeneration correlate with early disease progression (78). High presynaptic accumulation of insoluble α-syn has been proposed as a greater contributor to the development of clinical symptoms than LBs. Our proteomic (Fig. 4) and transcriptomic analyses (Fig. 5) suggest that mitochondrial defects are accompanied by an alteration of synapse-related RNA and protein levels. However, it remains unclear which pathways in the mitochondria-synapse signaling loop is dysregulated first by the formation and the maturation of α-syn pathological inclusions (79). Consistent with postmortem studies of PD patients (80, 81), during the transition from fibrils to LB-like inclusion, we showed a reduction of synaptic density, alterations of the protein level of both pre- and postsynaptic markers (Fig. 7), and dysregulation of the synaptic transcriptome (Fig. 5). Unlike mitochondrial dysfunction, which are manifested mainly once newly formed α-syn fibrils are reorganized into LB-like inclusions (D14 to D21), early synaptic changes at the transcriptomic level were observed concomitant with the beginning of the α-syn fibrillization process and the appearance of α-syn–seeded aggregates inside the neuritic extensions at the early stage of the seeding process (D4 to D7) (Fig. 5*A* and *SI Appendix*, Fig. S3 *A* and *B*). This suggests that synaptic dysfunction or different pathways linked to synaptic dysfunction are affected at the different stages of α-syn aggregation and LB formation and occur before the early onset of neurodegeneration, supporting the hypothesis that synaptopathy is an initial event in the pathogenesis of PD and related synucleinopathies (81, 82). Synaptotoxicity reflected by the down-regulation of the synaptic activity and the loss of synapses was also recently reported in seeding neuronal models (21, 70).

Finally, the ERK 1/2 signaling was also shown to be up-regulated during both the formation and the maturation of the LB-like inclusions (Fig. 7). The ERK 1/2 pathway regulates neuronal cell death, oxidative stress, mitochondria fission, and integrity, as well as synaptic plasticity (50), which are the major biological processes dysregulated in PD. Similar to what has been previously reported in bona fide LB from PD patients (52, 53), we found that p-ERK 1/2 was recruited inside the LB-like inclusions (*SI Appendix*, Fig. S12*C*). Therefore, dysregulation of this central signaling pathway during the formation and the maturation of the LB-like inclusions could affect mitochondrial and synaptic functions.

In conclusion, our work provides a comprehensive characterization of a highly reproducible neuronal model that recapitulates many of the key biochemical, structural, and organizational features of LB pathologies in PD brains. Using integrative imaging approaches, we were able to dissect the key processes involved the formation of LB-like pathologies and provide insight into their contribution to neuronal dysfunction and neurodegeneration. To our knowledge, this report is unique in showing the formation of organelle-rich LB-like inclusions in neurons and presents a comprehensive characterization of the different stages of LB formation, from seeding to fibrillization to the formation of LB-like inclusions at the molecular, biochemical, proteomic, transcriptomic, and structural levels. These advances, combined with the possibility to disentangle the three key processes (seeding, fibrillization, and LB formation) and investigate them separately, provide unique opportunities to: 1) Investigate the molecular mechanisms underpinning these processes, 2) elucidate their role in α-syn-induced toxicity and potential contributions to the pathogenesis of PD, and 3) screen for therapeutic agents based on the modulation of these pathways. The use of a model system that allows the investigation of these processes over a longer period of time (e.g., iPSC-derived neurons) could enable further insights into the molecular mechanisms that regulate LB pathology formation, maturation, and pathological diversity in PD and synucleinopathies (6), especially if the development of such model systems is driven by insight from human pathology.

Materials and Methods

Antibodies, compounds and the experimental procedures are described in *SI Appendix*.

Material and Data Availability. All experimental procedures and data are included in the article and in *SI Appendix*. Materials and protocols are available upon request from the corresponding author (H.L.).

ACKNOWLEDGMENTS. This work was supported by funding from Ecole Polytechnique Fédérale de Lausanne and UCB (Union Chimique Belge) pharma. We thank Firat Altay for the preparation of α-synuclein monomers and fibrils; and the Proteomics Core Facility, the Biomolecular Screening Core Facility, Gene Expression Core, and the Bio-imaging Core Facility (Ecole Polytechnique Fédérale de Lausanne) for their technical support and helpful discussions. Fig. 8 and *SI Appendix*, Fig. S10 *B–D* were created using BioRender.

1. C. Peng, R. J. Gathagan, V. M. Lee, Distinct α-synuclein strains and implications for heterogeneity among α-synucleinopathies. *Neurobiol. Dis.* **109**, 209–218 (2018).
2. W. Peelaerts, L. Bousset, V. Baekelandt, R. Melki, α-Synuclein strains and seeding in Parkinson's disease, incidental Lewy body disease, dementia with Lewy bodies and multiple system atrophy: Similarities and differences. *Cell Tissue Res.* **373**, 195–212 (2018).
3. L. S. Forno, Concentric hyalin intraneuronal inclusions of Lewy type in the brains of elderly persons (50 incidental cases): Relationship to parkinsonism. *J. Am. Geriatr. Soc.* **17**, 557–575 (1969).
4. L. S. Forno, L. E. DeLanney, I. Irwin, J. W. Langston, Electron microscopy of Lewy bodies in the amygdala-parahippocampal region. Comparison with inclusion bodies in the MPTP-treated squirrel monkey. *Adv. Neurol.* **69**, 217–228 (1996).
5. L. S. Forno, R. L. Norville, Ultrastructure of Lewy bodies in the stellate ganglion. *Acta Neuropathol.* **34**, 183–197 (1976).
6. G. M. Halliday, J. L. Holton, T. Revesz, D. W. Dickson, Neuropathology underlying clinical variability in patients with synucleinopathies. *Acta Neuropathol.* **122**, 187–204 (2011).
7. M. Goedert, R. Jakes, M. G. Spillantini, The synucleinopathies: Twenty years on. *J. Parkinsons Dis.* **7** (suppl. 1), S51–S69 (2017).
8. M. B. Fares *et al.*, Induction of de novo α-synuclein fibrillization in a neuronal model for Parkinson's disease. *Proc. Natl. Acad. Sci. U.S.A.* **113**, E912–E921 (2016).
9. A. Ulusoy, M. Decressac, D. Kirik, A. Björklund, Viral vector-mediated overexpression of α-synuclein as a progressive model of Parkinson's disease. *Prog. Brain Res.* **184**, 89–111 (2010).
10. M. Decressac, B. Mattsson, A. Björklund, Comparison of the behavioural and histological characteristics of the 6-OHDA and α-synuclein rat models of Parkinson's disease. *Exp. Neurol.* **235**, 306–315 (2012).
11. C. W. Shults, Lewy bodies. *Proc. Natl. Acad. Sci. U.S.A.* **103**, 1661–1668 (2006).
12. P. E. Duffy, V. M. Tennyson, Phase and electron microscopic observations of Lewy bodies and melanin granules in the substantia nigra and locus caeruleus in Parkinson's disease. *J. Neuropathol. Exp. Neurol.* **24**, 398–414 (1965).

NEUROSCIENCE
Downloaded at Palestinian Territory, occupied on December 1, 2021
www.manaraa.com

13. K. Hayashida, S. Oyanagi, Y. Mizutani, M. Yokochi, An early cytoplasmic change before Lewy body maturation: An ultrastructural study of the substantia nigra from an autopsy case of juvenile parkinsonism. *Acta Neuropathol.* **85**, 445–448 (1993).
14. H. Takahashi, K. Iwanaga, S. Egawa, F. Ikuta, Ultrastructural relationship between Lewy bodies and pale bodies studied in locus ceruleus neurons of a non-Parkinsonian patient. *Neuropathology* **14**, 73–80 (1994).
15. K. Wakabayashi *et al*., Accumulation of alpha-synuclein/NACP is a cytopathological feature common to Lewy body disease and multiple system atrophy. *Acta Neuropathol.* **96**, 445–452 (1998).
16. S. H. Shahmoradian *et al*., Lewy pathology in Parkinson's disease consists of crowded organelles and lipid membranes. *Nat. Neurosci.* **22**, 1099–1109 (2019).
17. S. Azeredo da Silveira *et al*., Phosphorylation does not prompt, nor prevent, the formation of alpha-synuclein toxic species in a rat model of Parkinson's disease. *Hum. Mol. Genet.* **18**, 872–887 (2009).
18. G. Taschenberger *et al*., Aggregation of αSynuclein promotes progressive in vivo neurotoxicity in adult rat dopaminergic neurons. *Acta Neuropathol.* **123**, 671–683 (2012).
19. L. W. Ko, H. H. Ko, W. L. Lin, J. G. Kulathingal, S. H. Yen, Aggregates assembled from overexpression of wild-type alpha-synuclein are not toxic to human neuronal cells. *J. Neuropathol. Exp. Neurol.* **67**, 1084–1096 (2008).
20. N. Ostrerova-Golts *et al*., The A53T alpha-synuclein mutation increases iron-dependent aggregation and toxicity. *J. Neurosci.* **20**, 6048–6054 (2000).
21. L. A. Volpicelli-Daley, K. C. Luk, V. M. Lee, Addition of exogenous α-synuclein preformed fibrils to primary neuronal cultures to seed recruitment of endogenous α-synuclein to Lewy body and Lewy neurite-like aggregates. *Nat. Protoc.* **9**, 2135–2146 (2014).
22. K. C. Luk, V. M. Lee, Modeling Lewy pathology propagation in Parkinson's disease. *Parkinsonism Relat. Disord.* **20** (suppl. 1), S85–S87 (2014).
23. W. P. Gai *et al*., In situ and in vitro study of colocalization and segregation of alpha-synuclein, ubiquitin, and lipids in Lewy bodies. *Exp. Neurol.* **166**, 324–333 (2000).
24. W. A. den Jager, Sphingomyelin in Lewy inclusion bodies in Parkinson's disease. *Arch. Neurol.* **21**, 615–619 (1969).
25. A.-L. Mahul-Mellier *et al*., The making of a Lewy body: The role of α-synuclein post-fibrillization modifications in regulating the formation and the maturation of pathological inclusions. bioRxiv:10.1101/500058 (19 December 2018).
26. J. P. Anderson *et al*., Phosphorylation of Ser-129 is the dominant pathological modification of alpha-synuclein in familial and sporadic Lewy body disease. *J. Biol. Chem.* **281**, 29739–29752 (2006).
27. M. Baba *et al*., Aggregation of alpha-synuclein in Lewy bodies of sporadic Parkinson's disease and dementia with Lewy bodies. *Am. J. Pathol.* **152**, 879–884 (1998).
28. W. Li *et al*., Aggregation promoting C-terminal truncation of alpha-synuclein is a normal cellular process and is enhanced by the familial Parkinson's disease-linked mutations. *Proc. Natl. Acad. Sci. U.S.A.* **102**, 2162–2167 (2005).
29. K. Prasad, T. G. Beach, J. Hedreen, E. K. Richfield, Critical role of truncated α-synuclein and aggregates in Parkinson's disease and incidental Lewy body disease. *Brain Pathol.* **22**, 811–825 (2012).
30. J. Tong *et al*., Brain alpha-synuclein accumulation in multiple system atrophy, Parkinson's disease and progressive supranuclear palsy: A comparative investigation. *Brain* **133**, 172–188 (2010).
31. E. Kuusisto, L. Parkkinen, I. Alafuzoff, Morphogenesis of Lewy bodies: Dissimilar incorporation of alpha-synuclein, ubiquitin, and p62. *J. Neuropathol. Exp. Neurol.* **62**, 1241–1253 (2003).
32. S. A. Tanik, C. E. Schultheiss, L. A. Volpicelli-Daley, K. R. Brunden, V. M. Lee, Lewy body-like α-synuclein aggregates resist degradation and impair macroautophagy. *J. Biol. Chem.* **288**, 15194–15210 (2013).
33. D. Grassi *et al*., Identification of a highly neurotoxic α-synuclein species inducing mitochondrial damage and mitophagy in Parkinson's disease. *Proc. Natl. Acad. Sci. U.S.A.* **115**, E2634–E2643 (2018).
34. K. Wakabayashi *et al*., The Lewy body in Parkinson's disease and related neurodegenerative disorders. *Mol. Neurobiol.* **47**, 495–508 (2013).
35. L. S. Forno, Lewy bodies. *N. Engl. J. Med.* **314**, 122 (1986).
36. K. Wakabayashi, H. Takahashi, S. Takeda, E. Ohama, F. Ikuta, Parkinson's disease: The presence of Lewy bodies in Auerbach's and Meissner's plexuses. *Acta Neuropathol.* **76**, 217–221 (1988).
37. M. R. Issidorides, C. Mytilineou, M. T. Panayotacopoulou, M. D. Yahr, Lewy bodies in parkinsonism share components with intraneuronal protein bodies of normal brains. *J. Neural Transm. Park. Dis. Dement. Sect.* **3**, 49–61 (1991).
38. T. E. Moors *et al*., The orchestration of subcellular alpha-synuclein pathology in the Parkinson's disease brain revealed by STED microscopy. bioRxiv:10.1101/470476 (10 May 2019).
39. K. Araki *et al*., Synchrotron FTIR micro-spectroscopy for structural analysis of Lewy bodies in the brain of Parkinson's disease patients. *Sci. Rep.* **5**, 17625 (2015).
40. J. E. Duda, B. I. Giasson, M. E. Mabon, V. M. Lee, J. Q. Trojanowski, Novel antibodies to synuclein show abundant striatal pathology in Lewy body diseases. *Ann. Neurol.* **52**, 205–210 (2002).
41. J. B. Leverenz *et al*., Proteomic identification of novel proteins in cortical Lewy bodies. *Brain Pathol.* **17**, 139–145 (2007).
42. Q. Xia *et al*., Proteomic identification of novel proteins associated with Lewy bodies. *Front. Biosci.* **13**, 3850–3856 (2008).
43. L. S. Forno, The Lewy body in Parkinson's disease. *Adv. Neurol.* **45**, 35–43 (1987).
44. M. F. Duffy *et al*., Quality over quantity: Advantages of using alpha-synuclein preformed fibril triggered synucleinopathy to model idiopathic Parkinson's disease. *Front. Neurosci.* **12**, 621 (2018).
45. J. T. Lamberts, P. Brundin, Axonal transport dysfunction in neurodegenerative diseases: The "holy grail" for developing disease modifying therapies? *Neurobiol. Dis.* **105**, 271–272 (2017).
46. P. E. Castillo, T. J. Younts, A. E. Chávez, Y. Hashimotodani, Endocannabinoid signaling and synaptic function. *Neuron* **76**, 70–81 (2012).
47. M. M. Monick *et al*., Constitutive ERK MAPK activity regulates macrophage ATP production and mitochondrial integrity. *J. Immunol.* **180**, 7485–7496 (2008).
48. C. N. Giachello *et al*., MAPK/Erk-dependent phosphorylation of synapsin mediates formation of functional synapses and short-term homosynaptic plasticity. *J. Cell Sci.* **123**, 881–893 (2010).
49. Y. Yamagata, A. C. Nairn, Contrasting features of ERK1/2 activity and synapsin I phosphorylation at the ERK1/2-dependent site in the rat brain in status epilepticus induced by kainic acid in vivo. *Brain Res.* **1625**, 314–323 (2015).
50. A. Bohush, G. Niewiadomska, A. Filipek, Role of mitogen activated protein kinase signaling in Parkinson's disease. *Int. J. Mol. Sci.* **19**, E2973 (2018).
51. N. Dzamko, J. Zhou, Y. Huang, G. M. Halliday, Parkinson's disease-implicated kinases in the brain; insights into disease pathogenesis. *Front. Mol. Neurosci.* **7**, 57 (2014).
52. J. H. Zhu, F. Guo, J. Shelburne, S. Watkins, C. T. Chu, Localization of phosphorylated ERK/MAP kinases to mitochondria and autophagosomes in Lewy body diseases. *Brain Pathol.* **13**, 473–481 (2003).
53. J. H. Zhu, S. M. Kulich, T. D. Oury, C. T. Chu, Cytoplasmic aggregates of phosphorylated extracellular signal-regulated protein kinases in Lewy body diseases. *Am. J. Pathol.* **161**, 2087–2098 (2002).
54. K. Afitska, A. Fucikova, V. V. Shvadchak, D. A. Yushchenko, α-Synuclein aggregation at low concentrations. *Biochim. Biophys. Acta. Proteins Proteom.* **1867**, 701–709 (2019).
55. M. B. Fares *et al*., The novel Parkinson's disease linked mutation G51D attenuates in vitro aggregation and membrane binding of α-synuclein, and enhances its secretion and nuclear localization in cells. *Hum. Mol. Genet.* **23**, 4491–4509 (2014).
56. J. Narkiewicz, G. Giachin, G. Legname, In vitro aggregation assays for the characterization of α-synuclein prion-like properties. *Prion* **8**, 19–32 (2014).
57. M. M. Wördehoff, W. Hoyer, α-Synuclein aggregation monitored by thioflavin T fluorescence assay. *Bio Protoc.* **8**, e2941 (2018).
58. R. J. Karpowicz , Jr, J. Q. Trojanowski, V. M. Lee, Transmission of α-synuclein seeds in neurodegenerative disease: Recent developments. *Lab. Invest.* **99**, 971–981 (2019).
59. K. Uryu *et al*., Convergence of heat shock protein 90 with ubiquitin in filamentous alpha-synuclein inclusions of alpha-synucleinopathies. *Am. J. Pathol.* **168**, 947–961 (2006).
60. T. Kanazawa *et al*., Three-layered structure shared between Lewy bodies and lewy neurites-three-dimensional reconstruction of triple-labeled sections. *Brain Pathol.* **18**, 415–422 (2008).
61. P. W. Lampert, A comparative electron microscopic study of reactive, degenerating, regenerating, and dystrophic axons. *J. Neuropathol. Exp. Neurol.* **26**, 345–368 (1967).
62. D. W. Dickson *et al*., Hippocampal degeneration differentiates diffuse lewy body disease (DLBD) from Alzheimer's disease: Light and electron microscopic immunocytochemistry of CA2-3 neurites specific to DLBD. *Neurology* **41**, 1402–1409 (1991).
63. E. Gómez-Tortosa, K. Newell, M. C. Irizarry, J. L. Sanders, B. T. Hyman, Alpha-synuclein immunoreactivity in dementia with Lewy bodies: Morphological staging and comparison with ubiquitin immunostaining. *Acta Neuropathol.* **99**, 352–357 (2000).
64. M. Sakamoto *et al*., Heterogeneity of nigral and cortical Lewy bodies differentiated by amplified triple-labeling for alpha-synuclein, ubiquitin, and thiazin red. *Exp. Neurol.* **177**, 88–94 (2002).
65. N. N. Vaikath *et al*., Heterogeneity in alpha-synuclein subtypes and their expression in cortical brain tissue lysates from Lewy body diseases and Alzheimer's disease. *Neuropathol. Appl. Neurobiol.* **45**, 597–608 (2019).
66. M. X. Henderson *et al*., Unbiased proteomics of early Lewy body formation model implicates active microtubule affinity-regulating kinases (MARKs) in synucleinopathies. *J. Neurosci.* **37**, 5870–5884 (2017).
67. L. Bedford *et al*., Depletion of 26S proteasomes in mouse brain neurons causes neurodegeneration and Lewy-like inclusions resembling human pale bodies. *J. Neurosci.* **28**, 8189–8198 (2008).
68. C. W. Olanow, D. P. Perl, G. N. DeMartino, K. S. McNaught, Lewy-body formation is an aggresome-related process: A hypothesis. *Lancet Neurol.* **3**, 496–503 (2004).
69. J. M. Froula *et al*., α-Synuclein fibril-induced paradoxical structural and functional defects in hippocampal neurons. *Acta Neuropathol. Commun.* **6**, 35 (2018).
70. Q. Wu *et al*., Alpha-synuclein (alphaSyn) preformed fibrils induce endogenous alphaSyn aggregation, compromise synaptic activity and enhance synapse loss in cultured excitatory hippocampal neurons. *J. Neurosci.* **39**, 5080–5094 (2019).
71. M. F. Beal, Mitochondria, oxidative damage, and inflammation in Parkinson's disease. *Ann. N. Y. Acad. Sci.* **991**, 120–131 (2003).
72. R. Betarbet, T. B. Sherer, D. A. Di Monte, J. T. Greenamyre, Mechanistic approaches to Parkinson's disease pathogenesis. *Brain Pathol.* **12**, 499–510 (2002).
73. X. Wang *et al*., Pathogenic alpha-synuclein aggregates preferentially bind to mitochondria and affect cellular respiration. *Acta Neuropathol. Commun.* **7**, 41 (2019).
74. V. Tapias *et al*., Synthetic alpha-synuclein fibrils cause mitochondrial impairment and selective dopamine neurodegeneration in part via iNOS-mediated nitric oxide production. *Cell. Mol. Life Sci.* **74**, 2851–2874 (2017).
75. A. Grünewald *et al*., Mitochondrial DNA depletion in respiratory chain-deficient Parkinson disease Neurons. *Ann. Neurol.* **79**, 366–378 (2016).
76. A. H. Schapira, Mitochondrial complex I deficiency in Parkinson's disease. *Adv. Neurol.* **60**, 288–291 (1993).
77. A. H. Schapira *et al*., Anatomic and disease specificity of NADH CoQ1 reductase (complex I) deficiency in Parkinson's disease. *J. Neurochem.* **55**, 2142–2145 (1990).
78. A. Bellucci *et al*., Review: Parkinson's disease: From synaptic loss to connectome dysfunction. *Neuropathol. Appl. Neurobiol.* **42**, 77–94 (2016).
79. M. Zaltieri *et al*., Mitochondrial dysfunction and α-synuclein synaptic pathology in Parkinson's disease: Who's on first? *Parkinsons Dis.* **2015**, 108029 (2015).
80. S. Zaja-Milatovic *et al*., Selective dendritic degeneration of medium spiny neurons in dementia with Lewy bodies. *Neurology* **66**, 1591–1593 (2006).
81. M. L. Kramer, W. J. Schulz-Schaeffer, Presynaptic alpha-synuclein aggregates, not Lewy bodies, cause neurodegeneration in dementia with Lewy bodies. *J. Neurosci.* **27**, 1405–1410 (2007).
82. J. C. Bridi, F. Hirth, Mechanisms of α-synuclein induced synaptopathy in Parkinson's disease. *Front. Neurosci.* **12**, 80 (2018).

Downloaded at Palestinian Territory, occupied on December 1, 2021

www.manaraa.com